The Journal of Chemical Physics

RESEARCH ARTICLE | NOVEMBER 15 2022

Quantification of electron correlation for approximate quantum calculations

Shunyue Yuan ; Yueqing Chang ; Lucas K. Wagner

J. Chem. Phys. 157, 194101 (2022)
https://doi.org/10.1063/5.0119260

The Journal of Chemical Physics ARTICLE scitation.org/journal/jcp

Quantification of electron correlation for approximate quantum calculations

Cite as: J. Chem. Phys. 157, 194101 (2022); doi: 10.1063/5.0119260
Submitted: 8 August 2022 • Accepted: 25 October 2022 •
Published Online: 15 November 2022

Shunyue Yuan, Yueqing Chang, and Lucas K. Wagner[a)]

AFFILIATIONS

Department of Physics, University of Illinois Urbana-Champaign, Champaign, Illinois 61801, USA

[a)]Author to whom correspondence should be addressed: lkwagner@illinois.edu

ABSTRACT

State-of-the-art many-body wave function techniques rely on heuristics to achieve high accuracy at an attainable computational cost to solve the many-body Schrödinger equation. By far, the most common property used to assess accuracy has been the total energy; however, total energies do not give a complete picture of electron correlation. In this work, we assess the von Neumann entropy of the one-particle reduced density matrix (1-RDM) to compare selected configuration interaction (CI), coupled cluster, variational Monte Carlo, and fixed-node diffusion Monte Carlo for benchmark hydrogen chains. A new algorithm, the circle reject method, is presented, which improves the efficiency of evaluating the von Neumann entropy using quantum Monte Carlo by several orders of magnitude. The von Neumann entropy of the 1-RDM and the eigenvalues of the 1-RDM are shown to distinguish between the dynamic correlation introduced by the Jastrow and the static correlation introduced by determinants with large weights, confirming some of the lore in the field concerning the difference between the selected CI and Slater–Jastrow wave functions.

I. INTRODUCTION

The development of computational algorithms to solve the many-electron problem is one of the grand challenges in modern physics, chemistry, and materials science. Such algorithms allow for accurate simulation of essentially all of chemistry and materials science, and indeed, a significant fraction of computer time is devoted to these simulations. By far, density functional theory (DFT) is the most common technique to achieve this goal; however, because of the unknown functional, it is difficult to systematically improve the performance despite significant attempts.[1–5] Wave function techniques, such as quantum Monte Carlo (QMC),[6,7] coupled cluster (CC),[8–10] density matrix renormalization group (DMRG),[11,12] or various truncated configuration interaction (CI) methods,[13–15] offer a systematically improvable path to accurate quantum simulations at the cost of larger computational expense compared with mean-field theories. Naïve methods such as exact diagonalization scale exponentially, in general; high accuracy at an attainable computational cost is only obtained using heuristics. For example, fixed-node diffusion Monte Carlo (FN-DMC) requires accurate wave function nodes, CC uses an exponential *ansatz*, and in CI methods, the determinants to be included must be selected.

It is interesting to compare the heuristic nature of many-electron algorithms to the no free lunch theorem[16] in optimization. Shortly stated, any two optimization algorithms are equivalent in performance when averaged across all possible problems. However, in practice, some optimization algorithms perform much better than others on problems in a given class. In many-electron simulations, we are concerned with problems that represent realistic physical situations, which is a very small subclass of all problems. While some many-body problems are provably computationally hard,[17] it is not always clear *a priori* which heuristics will lead to accurate and efficient solutions and how to assess different heuristics in a way that allows insight into how they treat electron correlation. The current state of the art focuses on total energy comparisons,[18] which, while important, often does not offer much insight into how the choice of approach affects the treatment of electron correlation.

There exist a number of approaches to quantify electronic correlation, each with its advantages and disadvantages. For example, the spatial entanglement[19] is closely related to the performance of DMRG;[20,21] however, it requires the replica trick in Monte Carlo,[22] which can be rather expensive computationally. Similarly, the two-particle reduced density matrix (2-RDM) is often too expensive to compute in its entirety. Hence, measures such as the cumulant

two-particle reduced density matrix[23] can be impractical for larger scale calculations. Other proposed measures[24,25] rely on the definition of a particular reference, which we did not find suitable for benchmarking across multiple methods. Finally, we should mention the idea of orbital-based entanglement measures,[26] which are well suited for understanding the DMRG[11] performance, but again require the 2-RDM. To compare disparate methods that may be under active development, it is critical that a quantification of correlation is very simple to evaluate.

In this work, we assess multipartite entanglement, defined as the von Neumann entropy of the one-particle reduced density matrix, as a tool to compare standard heuristics for treating electron correlation in many-particle wave functions, most significantly, quantum Monte Carlo approaches vs the selected configuration interaction approaches. We develop a new technique based on the rejection of eigenvalues, which improves the performance of Monte Carlo evaluations of the von Neumann entropy by several orders of magnitude. We find that the multipartite entanglement quantifies much of the current lore about how different wave function *ansatzes* add correlations. For example, Jastrow correlation factors are often said[27] to capture dynamic correlation, while configuration interaction with a few determinants captures static correlation. We use the von Neumann entropy of the one-particle reduced density matrix (1-RDM) to characterize electron correlation and find that the entropy of the 1-RDM correlates closely with these ideas.

II. MULTIPARTITE ENTANGLEMENT

We quantify the multipartite entanglement of a many-electron wave function Ψ using its 1-RDM

$$\rho_{ij,\sigma} = \langle \Psi | c^\dagger_{i\sigma} c_{j\sigma} | \Psi \rangle, \tag{1}$$

where $c^\dagger_{i\sigma}$ and $c_{i\sigma}$ are creation and annihilation operators for the single-particle orbital ϕ_i with spin σ. The entanglement entropy is defined as

$$s = -\operatorname{Tr}(\rho \ln \rho). \tag{2}$$

One can rewrite this using the entanglement spectrum, i.e., the eigenvalues of the 1-RDM, λ_i, as

$$s = -\sum_i \lambda_i \ln \lambda_i. \tag{3}$$

This quantity is closely related to the natural orbital occupation number commonly used in chemistry to characterize many-body wave functions.

The multipartite entanglement entropy measures how much information is lost when a single determinant is used to describe the wave function. It is monotonically related to the quasiparticle renormalization factor that appears in Fermi liquid theory, which also can be computed in quantum Monte Carlo as a measure of correlation.[28] As we shall show in this paper, the spectrum of the 1-RDM gives extra information about the type of correlation present in the wave function.

III. METHODS

A. Electronic structure methods

In this work, we performed calculations on one-dimensional chains of N equally spaced hydrogen atoms, where $N = 2, 4, 6, 8$, and 10. We consider systems with interatomic separation r equal to 1.4 and 3.0 in units of the Bohr radius $[a_B = \hbar^2/(me^2)]$ to compare weak and strong correlations. The ground-state wave functions were generated using Hartree–Fock (HF), heat-bath configuration interaction (HCI), coupled cluster with singles and doubles (CCSD), variational Monte Carlo (VMC), and fixed-node diffusion Monte Carlo (FN-DMC). The CCSD in H6 and smaller systems was performed using a correlation consistent 5-zeta valence basis set (cc-pV5Z). A correlation consistent triple-zeta valence basis set (cc-pVTZ)[29] was used for all other calculations.

We started by constructing HF and HCI wave functions. Each HCI wave function was specified by the threshold of the Hamiltonian matrix element ϵ_1, which controls which determinants are included.[15] We gradually decreased ϵ_1 until the energy converges. Due to limited computational resources, converged HCI wave functions were obtained only for hydrogen chains with $N \le 6$.

We used multi-determinant Slater–Jastrow (MSJ) wave functions to perform VMC and FN-DMC calculations. In the particular case of a single determinant, we will refer to the wave function as Slater–Jastrow (SJ). The SJ wave functions were constructed by multiplying the HF wave function by a two-body Jastrow factor e^U,[30]

$$\Psi_{\mathrm{SJ}} = e^U D^\uparrow[\phi_i(\mathbf{r}_j)] D^\downarrow[\phi_i(\mathbf{r}_j)]. \tag{4}$$

The MSJ wave functions are given by

$$\Psi_{\mathrm{MSJ}} = e^U \sum_{|c_\alpha| \le \epsilon_2} c_\alpha D^\uparrow_\alpha[\phi_i(\mathbf{r}_j)] D^\downarrow_\alpha[\phi_i(\mathbf{r}_j)], \tag{5}$$

where the determinants were taken from a HCI calculation with cutoff ϵ_1 and further selected by including only determinants with coefficients $|c_\alpha| \le \epsilon_2$. We used VMC to optimize the parameters in the Jastrow function U, the molecular orbitals $\{\phi_i\}$, and the determinant coefficients $\{c_\alpha\}$ and then applied FN-DMC to project out the ground state at a time step $\tau = 0.02\ \mathrm{Ha}^{-1}$.

Since the operator $\hat{\rho}$ does not commute with the Hamiltonian, we used the extrapolated estimator[7] to evaluate the 1-RDM of the fixed-node wave function Ψ_{FN},

$$\rho_{\mathrm{extrapolated}} = \rho_{\mathrm{mixed}} + \rho^\dagger_{\mathrm{mixed}} - \rho_{\mathrm{VMC}}, \tag{6}$$

where $\rho_{\mathrm{mixed}} = \langle \Psi_{\mathrm{FN}} | \hat{\rho} | \Psi_{\mathrm{T}} \rangle$ and $\rho_{\mathrm{VMC}} = \langle \Psi_{\mathrm{T}} | \hat{\rho} | \Psi_{\mathrm{T}} \rangle$. Here, $|\Psi_{\mathrm{T}}\rangle$ and $|\Psi_{\mathrm{FN}}\rangle$ are the optimized trial wave function and fixed-node wave function. To derive Eq. (6), we take $\delta\Psi = \Psi_{\mathrm{FN}} - \Psi_{\mathrm{T}}$ and only keep $\mathcal{O}(\delta\Psi)$,

$$\begin{aligned}\langle \Psi_{\mathrm{FN}} | \hat{\rho} | \Psi_{\mathrm{FN}} \rangle &= \langle (\Psi_{\mathrm{T}} + \delta\Psi) | \hat{\rho} | (\Psi_{\mathrm{T}} + \delta\Psi) \rangle \\ &\approx \langle \Psi_{\mathrm{T}} | \hat{\rho} | \Psi_{\mathrm{T}} \rangle + \langle \delta\Psi | \hat{\rho} | \Psi_{\mathrm{T}} \rangle + \langle \Psi_{\mathrm{T}} | \hat{\rho} | \delta\Psi \rangle \\ &= \langle \Psi_{\mathrm{FN}} | \hat{\rho} | \Psi_{\mathrm{T}} \rangle + \langle \Psi_{\mathrm{T}} | \hat{\rho} | \Psi_{\mathrm{FN}} \rangle - \langle \Psi_{\mathrm{T}} | \hat{\rho} | \Psi_{\mathrm{T}} \rangle.\end{aligned}$$

It is important that ρ_{mixed} and $\rho^\dagger_{\mathrm{mixed}}$ are evaluated using separate FN-DMC calculations in order for the circular distribution to be obeyed (Fig. 1) and thus for the circle reject algorithm to be applicable. If ρ_{mixed} and $\rho^\dagger_{\mathrm{mixed}}$ were from the same stochastic evaluation of

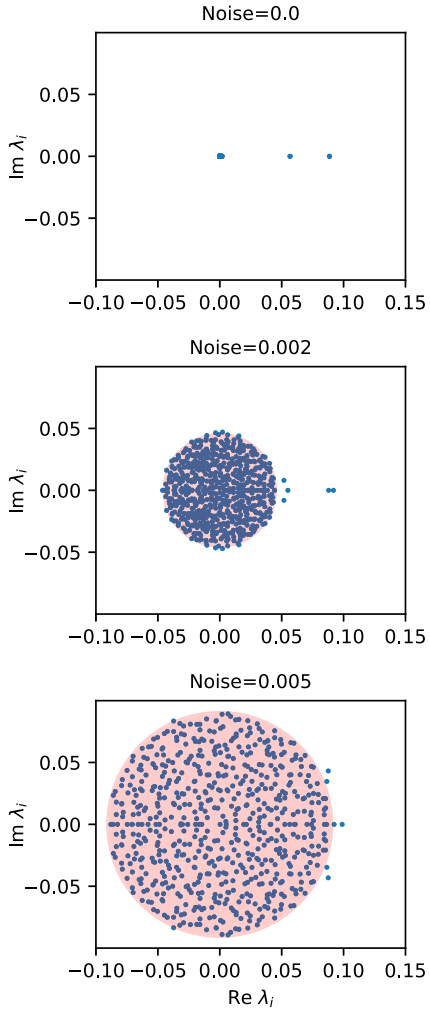

FIG. 1. The eigenvalues λ_i of the CCSD 1-RDM with added noise σ follow circular distribution.

the density matrix, the resulting extrapolated density matrix would be a mixture of symmetrized and non-symmetrized random matrices, which leads to a large bias in the estimated entropy as we will show in Sec. III B.

All quantum Monte Carlo (QMC) calculations were performed using the `PyQMC` package,[31] and the HF, HCI, and CCSD calculations were performed using the `PySCF` package.[32] We performed these calculations using a `Snakemake` workflow, which is available in the GitHub repository "Energy-Entropy."[33]

B. Computing the entanglement entropy for stochastic matrices: Circle reject algorithm

The entanglement entropy is biased when evaluated naïvely on a matrix with stochastic noise using Eq. (3). So it is necessary to develop a method to compute the entropy correctly from quantum Monte Carlo evaluations of the 1-RDM. Assume the true value of the 1-RDM is $\bar{A}$ and its quantum Monte Carlo evaluation is A with uncertainty ϵ; then, the probability density of A is

$$\rho(A|\bar{A},\epsilon) \propto \prod_{ij} \exp\left[\frac{(A_{ij}-\bar{A}_{ij})^2}{2\epsilon_{ij}^2}\right]. \tag{7}$$

We would like to evaluate the true von Neumann entropy

$$\bar{s} = -\sum_i \bar{\lambda}_i \ln \bar{\lambda}_i, \tag{8}$$

where $\bar{\lambda}_i$ are the eigenvalues of the matrix $\bar{A}$.

Our objective is to infer, from A, the most probable values of $\bar{\lambda}_i$ and, therefore, $\bar{s}$. One complication is that most physical 1-RDMs have only a few non-zero eigenvalues; most are close to 1 or 0. In contrast, a random positive definite matrix has eigenvalues that almost always deviate from 0 to 1. For the part of the 1-RDM that is zero, the stochastic noise brought by QMC distribute eigenvalues uniformly in a circle,[34] which gives rise to a bias in the computed entropy.

To illustrate the distribution of eigenvalues of noisy matrices, we added Gaussian noise with standard deviation σ to each element of the 1-RDM: $A_{ij} = \bar{A}_{ij} + \chi_{ij}$, $\chi_{ij} \sim \mathcal{N}(0,\sigma)$, where $\bar{A}$ was computed using the CCSD for H6 at a 3.0 a_B separation and a cc-pV5Z basis set. Figure 1 shows the eigenvalues of the matrix A with standard deviation $\sigma = 0.0, 0.002$, and 0.005, where the coordinates represent the real and imaginary parts of the eigenvalues. The red circles on the plot have radii $\sigma\sqrt{N}$, where N is the size of the matrix. The noise in the eigenvalue spectrum is covered by the red circles, given by random matrix theory.[34] If all the eigenvalues with noise 0.002 and 0.005 were included to evaluate the von Neumann entropy using Eq. (3), the resultant entropy would be biased from the zero-noise value.

We considered the following three strategies of reducing the bias in entropy naïvely computed using Eq. (3) due to the presence of noise, shown in Fig. 2(a).

1. **Symmetrize the matrix** by diagonalizing $\frac{A+A^\dagger}{2}$.
2. **Enforce positivity** by diagonalizing A and setting all negative eigenvalues to zero, and all imaginary components to zero.
3. **Circle reject** by removing all eigenvalues within the circular distribution given in red in Fig. 1.

In Fig. 2, we show the bias in the entropy as a function of noise σ added to a CCSD 1-RDM. It is clear from the figure that the circle reject algorithm (noted by the upper and lower bounds) has a dramatically lower bias than the other strategies.

Our best strategy is the circle reject algorithm, which we give in detail here. The strategy is as follows:

1. Compute the eigenvalues λ_i of matrix A.
2. Estimate the radius $r = \sigma\sqrt{N}$ of the circle.
3. Adjust the radius as

$$r' = \max(\{|\lambda_i| : |\lambda_i| > r,\ |\mathrm{Re}(\lambda_i)| < r\})(1+\delta).$$

4. Compute the first estimate of entropy as

$$S = -\textstyle\sum_{|\lambda_i|\geq r'} \lambda_i \ln \lambda_i.$$

5. Estimate the upper and lower bounds of entropy using Eqs. (10) and (12).

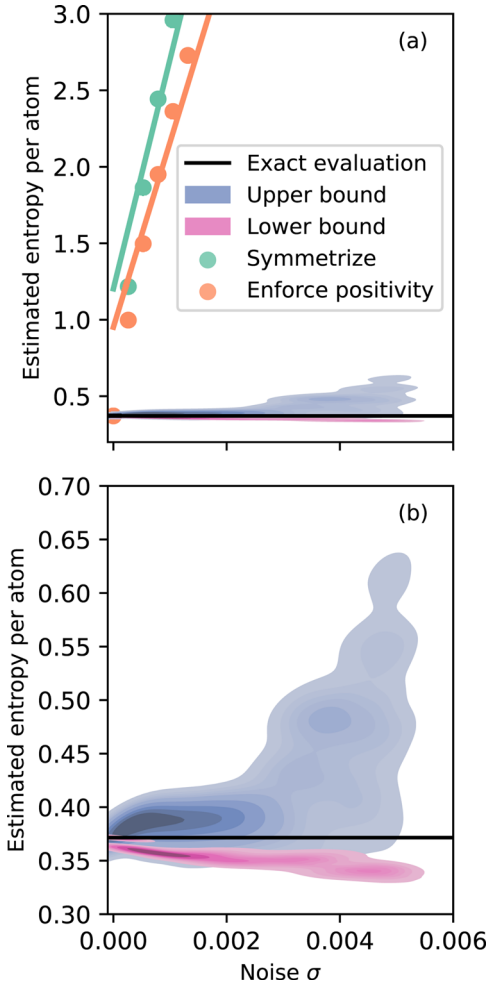

FIG. 2. (a) Estimated entropy per atom using different strategies vs the noise added to a CCSD 1-RDM. The circle reject technique corrects the bias in the entropy due to statistical fluctuations. The upper (lower) bound of entropy was estimated from the missing trace and bounds above (below) the exact result. (b) Zoomed-in circle reject estimations shown in (a).

We found that step 3 improved the performance of the algorithm, since occasionally, the noise falsely brings some small eigenvalues out of the circle with radius r. Step 3 makes sure these eigenvalues are rejected. We found that using an empirical value of 0.01 for the parameter δ yields reasonable estimates of the entropy in step 4.

In step 5, the upper and lower bounds are estimated by distributing the missing trace due to rejection in different ways. The total trace of the 1-RDM should be N, where N is the number of electrons; however, there is usually a small remainder due to the fact that the circle rejection removes some small eigenvalues as an unwanted side effect. If the remaining trace were ignored, the estimated entropy would be a lower bound. Because the remaining trace is below the estimated circle distribution, we do not know how the eigenvalues are distributed; however, we show how to establish approximate bounds on the entropy.

Rather than rejecting the eigenvalues, we obtain a tighter lower bound as follows. We equally re-distribute the missing trace among m eigenvalues in a minimum entropy way, which is the fewest number of maximal eigenvalues that would have been rejected by the algorithm. We distribute the eigenvalues such that they are just below the rejection radius r', i.e.,

$$\lambda_1 = \frac{N - \sum_{|\lambda_i| \geq r'} \lambda_i}{m},$$
$$m = \left\lceil \frac{N - \sum_{|\lambda_i| \geq r'} \lambda_i}{r'} \right\rceil, \tag{9}$$

where $\lceil\,\rceil$ indicates the smallest integer greater than the argument, and λ_i are the eigenvalues of the QMC 1-RDM. We compute the lower bound as

$$S_1 = -\sum_{|\lambda_i| \geq r'} \lambda_i \ln \lambda_i - m\lambda_1 \ln \lambda_1. \tag{10}$$

To estimate the upper bound of the entropy, we equally redistribute the missing trace among all the rejected eigenvalues. This is the maximum entropy that the missing trace could contribute to the total,

$$\lambda_u = \frac{N - \sum_{|\lambda_i| \geq r'} \lambda_i}{n}, \tag{11}$$

where n is the total number of eigenvalues that are rejected. Then, the approximate upper bound is

$$S_u = -\sum_{|\lambda_i| \geq r'} \lambda_i \ln \lambda_i - n\lambda_u \ln \lambda_u. \tag{12}$$

Figure 2 shows that the circle reject algorithm is much more efficient for the 1-RDM with Gaussian noise than the other two strategies we considered. The lower bound derived is always a strict lower bound, but the upper bound occasionally falls below the true value. The upper bound fails when a statistical fluctuation results in an enhancement of the eigenvalues outside the circle reject radius so that the maximum missing entropy is underestimated. For the rest of the paper, the estimated upper and lower bounds will be reported in all estimations of the entropy using stochastic methods (VMC and DMC), *in lieu* of single-σ uncertainties.

The scaling of the entropy calculation using the circle reject algorithm is $\mathcal{O}(N^3)$, where N is some number indicating the system size. The evaluation of the 1-RDM per MC sweep is $\mathcal{O}(N_b^2)$, where N_b is the number of basis functions. Since the radius grows as $\sqrt{N_b}$, one needs to perform a number of sweeps proportional to N_b to keep the radius constant, resulting in a scaling of $\mathcal{O}(N_b^3)$, the same as the total energy calculation for a constant error on the total energy. In practice, we find that the evaluation of the 1-RDM does not add a large cost to an energy-only calculation.

IV. RESULTS

First, we check the energy convergence of our high accuracy calculations. Figure 3 shows the ground state energies obtained using different methods (HCI, CCSD, VMC, and FN-DMC) vs the number of determinants for a strongly correlated system H6, $r = 3.0a_B$. Similar results were also obtained for weakly correlated systems; data

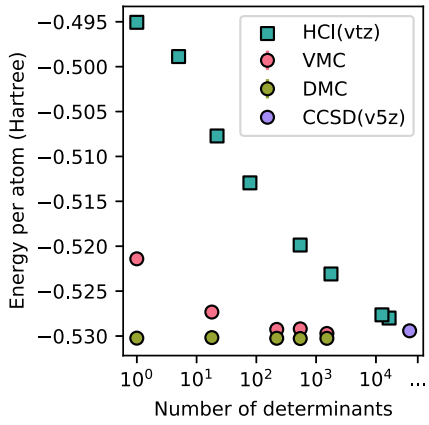

FIG. 3. (H6, r = 3.0a_B) The energies computed using HCI wave functions (obtained using cc-pVTZ basis), VMC and FN-DMC (time step = 0.02) with SJ and MSJ wave functions, and CCSD (with cc-pV5Z basis) vs the number of determinants. The energies obtained agree across different methods, as the number of determinants increases.

are available in the repository.[33] Figure 3 shows that the energies computed using the FN-DMC approach yield near-exact energies with a small number of determinants. The energies computed using VMC, FN-DMC, and CCSD agree well as the number of determinants increases. The converged HCI energy is quite close to the FN-DMC and CCSD energies; however, note that we could only afford to perform converged HCI calculations at the triple-zeta level of basis.

In Fig. 4, we compare the energy and entropy of wave function methods as they converge toward the exact ground state for the weakly correlated $r = 1.4a_B$ interatomic separation. Like the energy, the entropy converges to a similar value for different methods. As one might expect for weak correlation, we find that in this case, the Jastrow factor and DMC, in general, are highly effective in describing the entropy of the system regardless of the number of determinants in the wave function.

In Fig. 5, we compare the energy and entropy of wave function methods as they converge toward the exact ground state for the strongly correlated $r = 3.0a_B$ interatomic separation. Similar to the weakly correlated systems, FN-DMC with MSJ wave functions

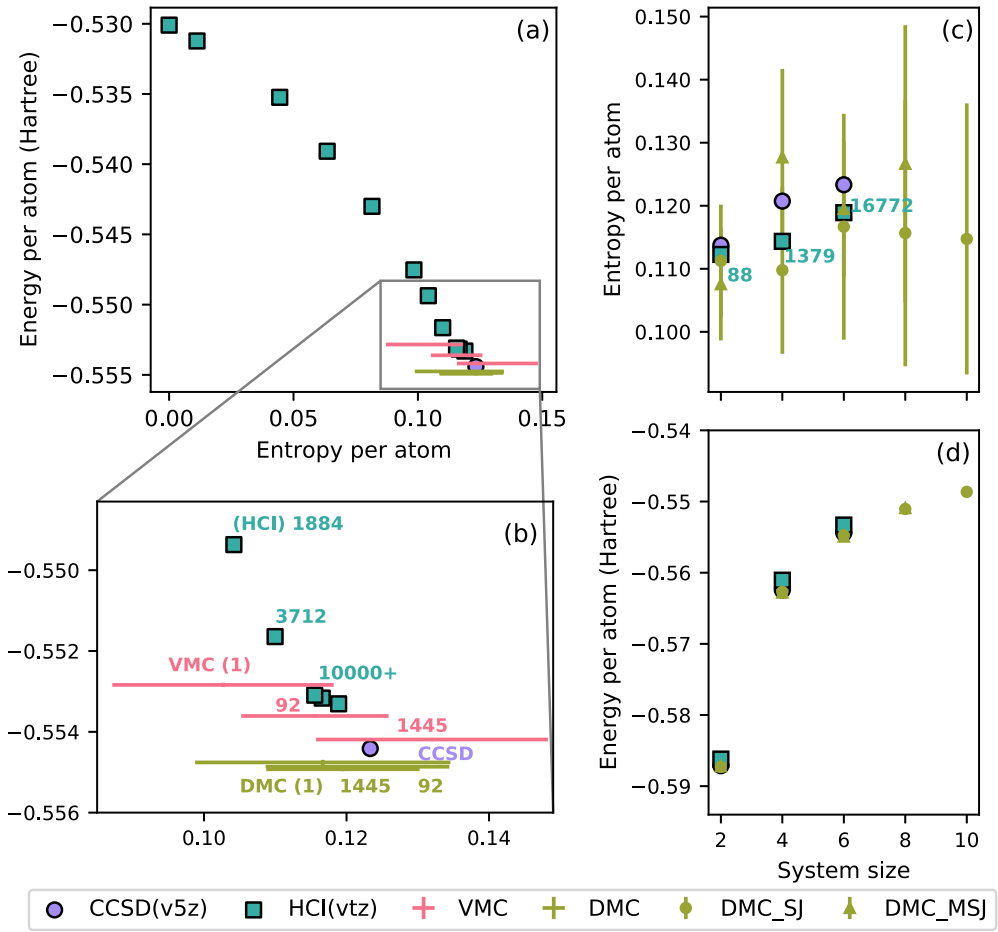

FIG. 4. (a) Converged ground state energy vs entropy per atom for a weakly correlated system (H6, $r = 1.4a_B$), computed using CCSD (with cc-pV5Z basis), HCI wave functions (with cc-pVTZ basis), and VMC and FN-DMC using SJ and MSJ trial wave functions. (b) Zoomed-in lower-right portion of (a). The numbers next to each point denote the numbers of determinants selected in the corresponding optimized wave functions. The edges of the bars on the VMC or FN-DMC points represent the lower and upper bounds computed following the method described in Sec. III B. (c) The scaling of entropy per atom with system size for weakly correlated systems ($r = 1.4a_B$). The number of determinants included in the converged HCI wave functions is annotated. (d) The scaling of energy per atom with system size for weakly correlated systems ($r = 1.4a_B$).

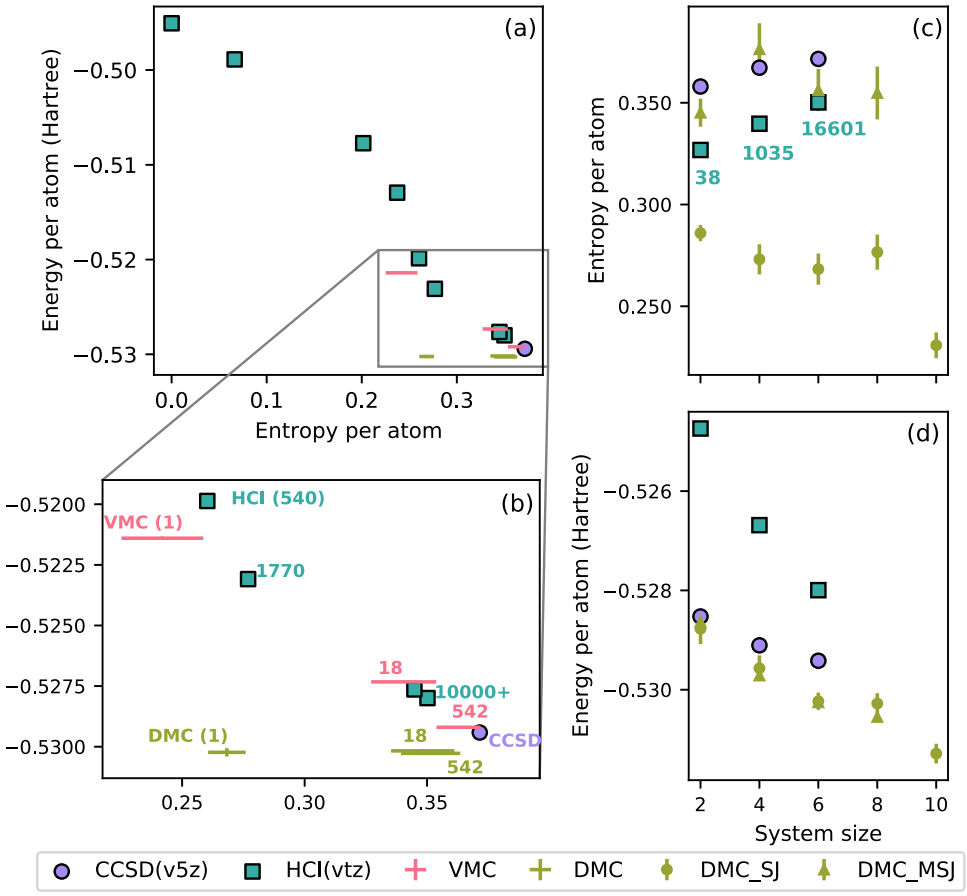

FIG. 5. (a) Converged ground state energy vs entropy per atom for a strongly correlated system (H6, $r = 3.0a_B$), computed using CCSD (with cc-pV5Z basis), HCI wave functions (with cc-pVTZ basis), and VMC and FN-DMC using SJ and MSJ trial wave functions. (b) Zoomed-in lower-right portion of (a). The numbers next to each point denote the numbers of determinants selected in the corresponding optimized wave functions. The edges of the bars on the VMC or FN-DMC points represent the lower and upper bounds computed following the method described in Sec. III B. (c) The scaling of entropy per atom with system size for strongly correlated systems ($r = 3.0a_B$). The number of determinants included in the converged HCI wave functions is annotated. (d) The scaling of energy per atom with system size for strongly correlated systems ($r = 3.0a_B$).

is highly effective in describing the entropy of the system regardless of the number of determinants in the wave function. Unlike weakly correlated systems in which the dynamic correlation is dominant, in strongly correlated systems, FN-DMC with SJ wave functions results in energies very close to those computed using MSJ wave functions, but misses a part of the entropy, which corresponds to the static correlation.

The difference in how the methods add correlation aligns with the ideas of dynamic and static correlations often discussed in the quantum chemistry literature. Dynamic correlation is identified as originating from a large set of determinants $D_\alpha^{\uparrow,\downarrow}$ with small coefficients c_α. Dynamic correlation corresponds to the perturbative behavior that can be captured from a qualitatively correct, effective one-body reference state. Static correlation is identified from a small number of determinants $D_\alpha^{\uparrow,\downarrow}$ with sizable coefficients c_α toward the full many-body expansion.[35]

We further look into the entanglement spectrum (difference between the eigenvalues of the 1-RDM and those of an idempotent matrix [the 1-RDM of a non-interacting system]) for a strongly correlated system (H6, $r = 3.0a_B$) shown in Fig. 6. This figure mainly gives us 3 pieces of information. The selected CI and Jastrow factors are complementary in their treatment of correlation. The selected CI wave functions first include the static correlation, then add more dynamic correlation, and treat the static correlation more accurately as the expansion approaches convergence. The Jastrow factor allows VMC and FN-DMC to treat dynamic correlation more efficiently with fewer number of determinants compared with selected CI.

First, when a SJ wave function performed using VMC obtains approximately the same entropy as a HCI wave function does, they primarily treat different types of correlations. In Fig. 6, the entropies computed using the HCI wave function with only 78 determinants (HCI@78) and the VMC single-determinant SJ wave function (VMC-SJ) are approximately the same. The entanglement spectrum of HCI@78 shows more evident static correlation, as 2 of its eigenvalues of ρ differ significantly from those of an idempotent matrix. On the other hand, the VMC-SJ primarily describes dynamic correlation, as it has most of the eigenvalues closer to those of an idempotent matrix. This information implies that the Jastrow factor reduces the wave function energy by including more dynamic correlation, which is equivalent to adding small components of high-energy determinants into the wave function. Meanwhile, when reducing the wave function energy, the HCI primarily treats static correlation by truncating determinants with small coefficients. This observation supports the idea that selected CI and Jastrow factors are complementary in their treatment of correlation.[36–38]

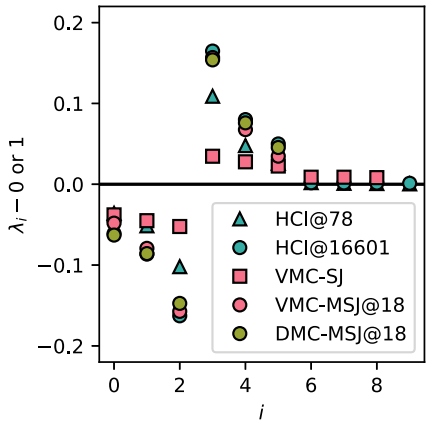

FIG. 6. The entanglement spectrum of a strongly correlated system (H6, $r = 3.0a_B$), computed using HCI wave functions with different number of determinants, VMC using optimized SJ and MSJ wave functions, and FN-DMC with MSJ trial wave functions. The numbers of determinants included in the wave functions are labeled after the names of the methods. The sorted eigenvalues λ_i of the 1-RDMs (for spin up) minus either 0 or 1 are plotted against the index i of the eigenvalues. Only the ten largest eigenvalues are shown.

Second, a converged HCI wave function treats both dynamic correlation and static correlation better than an unconverged HCI wave function. Correspondingly, the converged HCI wave function has a larger entropy than the unconverged one. For the system shown in Fig. 6, the HCI wave function converges when using 16 601 determinants (HCI@16601). Compared with the ρ of HCI@78 that has only a few non-zero eigenvalues, the ρ of HCI@16601 has many small eigenvalues, which are omitted in the figure. In addition, the first few eigenvalues of HCI@78 are closer to those of an idempotent matrix than those of HCI@16601. This information implies that when CI wave functions approach convergence, they add more dynamic correlation and also treat static correlation more accurately.

Third, the FN-DMC treats the correlation efficiently using a trial wave function with only a few optimized determinants from a converged HCI wave function. As shown in Fig. 6, the entanglement spectra of DMC-MSJ@18 and HCI@16601 are very similar. The trial wave function used in the DMC-MSJ is optimized with only 18 out of 16601 determinants computed by the HCI wave function, but the DMC-MSJ obtains almost the same entropy as the HCI wave function.

V. CONCLUSION

In conclusion, we used multipartite entanglement and its spectrum to evaluate the differences between quantum chemistry and quantum Monte Carlo approaches to the treatment of electron correlation. We developed a new algorithm, the circle reject method, to evaluate the entropy of randomized matrices, which enabled an accurate evaluation of this quantity using the quantum Monte Carlo. We found that the Jastrow factor, indeed, appears to mainly add dynamic correlation by creating many small eigenvalues of the 1-RDM, while selected CI methods tend to create a few large eigenvalues first, which is an explicit observation of the complementary nature of these terms in the wave function.

The circle reject algorithm could find more uses, as the use of stochastic algorithms in quantum chemistry appears to be increasing.[39] It is particularly worth using if a matrix is likely to have very few non-zero eigenvalues but is evaluated stochastically. Other methods along similar lines could potentially be developed; the key insight is to recognize prior knowledge about the output of a given function. In this way, the circle reject algorithm is similar strategically to the maximum entropy principle,[40] although with a different set of assumptions.

The eigenvalues of the 1-RDM are simple to compute, and we believe that it should become more standard to evaluate multipartite entanglement as a measure of electronic correlation. Such a measure also allows one to make contact with the roughly equivalent homogeneous electron gas, since the momentum distribution is known for several values of r_s.[28]

SUPPLEMENTARY MATERIAL

See the supplementary material for a comma separated values file containing all the data presented in the manuscript.

ACKNOWLEDGMENTS

L.K.W. was supported by the U.S. National Science Foundation via Award No. 1931258 to implement the methodology in the `PyQMC` project. Y.C. was supported by the U.S. Department of Energy, Office of Science, Office of Basic Energy Sciences, Computational Materials Sciences Program, under Award No. DE-SC0020177 to assist with the analysis and writing of the manuscript. This work made use of the Illinois Campus Cluster, a computing resource that is operated by the Illinois Campus Cluster Program (ICCP) in conjunction with the National Center for Supercomputing Applications (NCSA) and that is supported by funds from the University of Illinois at Urbana-Champaign.

AUTHOR DECLARATIONS

Conflict of Interest

The authors have no conflicts to disclose.

Author Contributions

Shunyue Yuan: Data curation (equal); Investigation (equal); Methodology (equal); Project administration (equal); Visualization (equal); Writing – original draft (equal); Writing – review & editing (equal). **Yueqing Chang**: Visualization (equal); Writing – review & editing (equal). **Lucas K. Wagner**: Conceptualization (equal); Formal analysis(equal); Funding acquisition (equal); Methodology (equal); Project administration (equal); Software (equal); Supervision (equal); Writing – review & editing (equal).

DATA AVAILABILITY

The data that support the findings of this study are available within the article and its supplementary material.[33]

APPENDIX: ANOTHER QUANTITY TO MEASURE CORRELATIONS: THE DEVIATION FROM IDEMPOTENCE

We computed another quantity to measure the correlations of wave functions, as proposed by Ref. 41,

$$\Lambda = \mathrm{Tr}(\rho - \rho^2). \tag{A1}$$

For an uncorrelated wave function, the 1-RDM is idempotent, i.e., $\rho = \rho^2$, $\Lambda = 0$. Thus, this quantity can be viewed as a deviation from idempotence.

Figure 7 shows that the entropy and the deviation from idempotence Λ show similar dependence on energy. The shape of the data distribution for the deviation from idempotence is slightly more spread out than that of the entropy, as they have different metrics and units. While the deviation from idempotence is easier to evaluate and less susceptible to the stochastic errors in QMC methods, the von Neumann entropy gives more information about correlation through entanglement spectrum, as shown in Fig. 6.

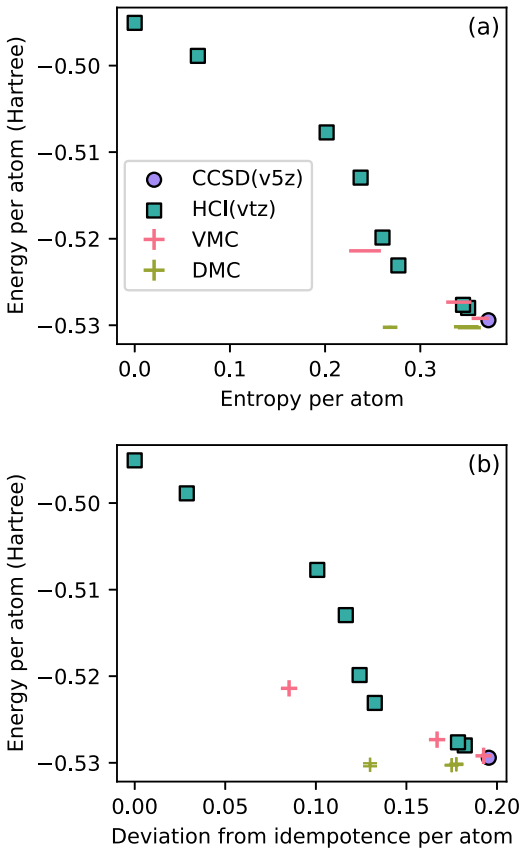

FIG. 7. Entropy and deviation from idempotence show similar dependence on energy. The calculations were performed in a strongly correlated system (H6, $r = 3.0a_B$), using CCSD (with cc-pV5Z basis), HCI wave functions (with cc-pVTZ basis) using different number of determinants, and VMC and FN-DMC using SJ and MSJ trial wave functions. (a) Energy vs entropy per atom. The edges of the bars on the VMC or FN-DMC points represent the lower and upper bounds computed following the method described in Sec. III B. (b) Energy vs the deviation from idempotence per atom. The VMC or FN-DMC points are represented using plus marks. The upper and lower bounds were not evaluated.

REFERENCES

[1] J. Sun, A. Ruzsinszky, and J. Perdew, Phys. Rev. Lett. **115**, 036402 (2015).
[2] J. Sun, R. C. Remsing, Y. Zhang, Z. Sun, A. Ruzsinszky, H. Peng, Z. Yang, A. Paul, U. Waghmare, X. Wu, M. L. Klein, and J. P. Perdew, Nat. Chem. **8**, 831 (2016).
[3] M. A. Morales, J. R. Gergely, J. McMinis, J. M. McMahon, J. Kim, and D. M. Ceperley, J. Chem. Theory Comput. **10**, 2355 (2014).
[4] P. Borlido, T. Aull, A. W. Huran, F. Tran, M. A. L. Marques, and S. Botti, J. Chem. Theory Comput. **15**, 5069 (2019).
[5] P. Borlido, J. Schmidt, A. W. Huran, F. Tran, M. A. L. Marques, and S. Botti, npj Comput. Mater. **6**, 96 (2020).
[6] D. M. Ceperley and B. J. Alder, Phys. Rev. Lett. **45**, 566 (1980).
[7] W. M. C. Foulkes, L. Mitas, R. J. Needs, and G. Rajagopal, Rev. Mod. Phys. **73**, 33 (2001).
[8] J. Cizek and J. Paldus, Phys. Scr. **21**, 251 (1980).
[9] J. Paldus, J. Čížek, and B. Jeziorski, J. Chem. Phys. **90**, 4356 (1989).
[10] R. J. Bartlett and M. Musiał, Rev. Mod. Phys. **79**, 291 (2007).
[11] S. R. White, Phys. Rev. Lett. **69**, 2863 (1992).
[12] U. Schollwöck, Rev. Mod. Phys. **77**, 259 (2005).
[13] B. Huron, J. P. Malrieu, and P. Rancurel, J. Chem. Phys. **58**, 5745 (1973).
[14] R. Cimiraglia and M. Persico, J. Comput. Chem. **8**, 39 (1987).
[15] A. A. Holmes, N. M. Tubman, and C. J. Umrigar, J. Chem. Theory Comput. **12**, 3674 (2016).
[16] D. H. Wolpert and W. G. Macready, IEEE Trans. Evol. Comput. **1**, 67 (1997).
[17] M. Troyer and U.-J. Wiese, Phys. Rev. Lett. **94**, 170201 (2005).
[18] Simons Collaboration on the Many-Electron Problem, K. T. Williams, Y. Yao, J. Li, L. Chen, H. Shi, M. Motta, C. Niu, U. Ray, S. Guo, R. J. Anderson, J. Li, L. N. Tran, C.-N. Yeh, B. Mussard, S. Sharma, F. Bruneval, M. van Schilfgaarde, G. H. Booth, G. K.-L. Chan, S. Zhang, E. Gull, D. Zgid, A. Millis, C. J. Umrigar, and L. K. Wagner, Phys. Rev. X **10**, 011041 (2020).
[19] L. Amico, R. Fazio, A. Osterloh, and V. Vedral, Rev. Mod. Phys. **80**, 517 (2008).
[20] G. Vidal, Phys. Rev. Lett. **91**, 147902 (2003).
[21] G. Vidal, Phys. Rev. Lett. **93**, 040502 (2004).
[22] J. McMinis and N. M. Tubman, Phys. Rev. B **87**, 081108 (2013).
[23] T. Juhász and D. A. Mazziotti, J. Chem. Phys. **125**, 174105 (2006).
[24] L. Delle Site, Int. J. Quantum Chem. **115**, 1396 (2015).
[25] E. Ramos-Cordoba, P. Salvador, and E. Matito, Phys. Chem. Chem. Phys. **18**, 24015 (2016).
[26] K. Boguslawski, P. Tecmer, Ö. Legeza, and M. Reiher, J. Phys. Chem. Lett. **3**, 3129 (2012).
[27] C. Filippi and C. J. Umrigar, J. Chem. Phys. **105**, 213 (1996).
[28] M. Holzmann, B. Bernu, C. Pierleoni, J. McMinis, D. M. Ceperley, V. Olevano, and L. Delle Site, Phys. Rev. Lett. **107**, 110402 (2011).
[29] T. H. Dunning, J. Chem. Phys. **90**, 1007 (1989).
[30] L. K. Wagner, M. Bajdich, and L. Mitas, J. Comput. Phys. **228**, 3390 (2009).
[31] See https://github.com/WagnerGroup/pyqmc for PyQMC: Python library for real space quantum Monte Carlo.
[32] Q. Sun, T. C. Berkelbach, N. S. Blunt, G. H. Booth, S. Guo, Z. Li, J. Liu, J. D. McClain, E. R. Sayfutyarova, S. Sharma, S. Wouters, and G. K. L. Chan, Wiley Interdiscip. Rev.: Comput. Mol. Sci. **8**, e1340 (2017).
[33] See https://github.com/WagnerGroup/Energy-Entropy/tree/clean_for_paper for Snakemake workflow and data.
[34] J. Ginibre, J. Math. Phys. **6**, 440 (1965).

[35]C. Mejuto Zaera, "Strong correlation through selected configuration interaction: From molecules to extended systems," Ph.D. dissertation (University of California, Berkeley, 2021).
[36]M. Dash, S. Moroni, A. Scemama, and C. Filippi, J. Chem. Theory Comput. **14**, 4176 (2018).
[37]M. Dash, J. Feldt, S. Moroni, A. Scemama, and C. Filippi, J. Chem. Theory Comput. **15**, 4896 (2019).
[38]M. Dash, S. Moroni, C. Filippi, and A. Scemama, J. Chem. Theory Comput. **17**, 3426 (2021).
[39]M. A. Morales-Silva, K. D. Jordan, L. Shulenburger, and L. K. Wagner, J. Chem. Phys. **154**, 170401 (2021).
[40]E. T. Jaynes, Phys. Rev. **106**, 620 (1957).
[41]L. Muechler, D. I. Badrtdinov, A. Hampel, J. Cano, M. Rösner, and C. E. Dreyer, Phys. Rev. B **105**, 235104 (2022).